Coexistence of the Franz-Keldysh and Wannier-Stark effect in semiconductor superlattices

Norbert Linder, Klaus H. Schmidt, Wolfgang Geisselbrecht, and Gottfried H. Döhler
Institut für Technische Physik I, Universität Erlangen-Nürnberg, Erwin-Rommel-Strasse 1, 91058 Erlangen, Germany

Holger T. Grahn and Klaus Ploog
Paul-Drude-Institut für Festkörperelektronik, Hausvogteiplatz 5-7, 10117 Berlin, Germany

Harald Schneider
Fraunhofer-Institut für Angewandte Festkörperphysik, Tullastrasse 72, 79108 Freiburg, Germany
(Received 30 May 1995)

The optical absorption of short-period semiconductor superlattices with an electric field perpendicular to the layer plane is studied. The applied fields cover the range from the "miniband regime" (low fields), where Franz-Keldysh (FK) oscillations can be observed, up to the regime of Wannier-Stark (WS) transitions (high fields). Special emphasis is devoted to the investigation of the intermediate-field regime where both effects are present. We give a thorough theoretical treatment which is the basis for results published recently. It is shown that the crystal momentum representation can correctly describe the absorption behavior over the whole field range. For intermediate fields one obtains complicated but regular structures due to the coexistence of WS transitions and FK oscillations. Using double differential photocurrent spectroscopy, a technique of modulation spectroscopy, we have investigated a strongly coupled GaAs/AlAs superlattice. A symmetric fan of negative *and* positive WS transitions and a series of FK oscillations both near the lower and the upper combined miniband edge could be observed with unprecedented resolution. The theoretical results are confirmed excellently.

I. INTRODUCTION

Electro-optical effects in semiconductor superlattices are a field of continuing interest, both because of the implications for attractive device applications and insight into basic principles of solid state physics. The latter is the topic of this paper. Basically there are two major effects in the electroabsorption characteristics of any periodic semiconductor system with direct band gap, no matter whether it is a natural or an artificial crystal: the Franz-Keldysh (FK) and the Wannier-Stark (WS) effect.

The Franz-Keldysh effect is well known for bulk material since the early days of solid state physics. In 1958 Franz and Keldysh[2] independently found that there should be an exponentially decaying absorption tail for photon energies smaller than the band gap energy if an electric field is superimposed on the crystal potential. A few years later Aspnes[3,4] extended their results on the photon energy range above the band gap energy and demonstrated that characteristic oscillations of the absorption coefficient around the zero-field value, the so-called Franz-Keldysh oscillations, should occur. This behavior was expected to appear in the vicinity of any Van Hove singularity in the Brillouin zone of a crystal. Magnitude and period of the FK oscillations should increase with increasing field. In the following years, the FK effect could be observed experimentally and the theoretical predictions were excellently confirmed.[5] Apart from some corrections, due to the complicated band structure of real crystals,[6] the effect is now well understood and has found a wide range of applications in the determination of critical point energies in crystal band structures and electric fields in semiconductor structures.

The derivation of the expression for the FK absorption assumed infinitely extended bands resulting in a continuous energy spectrum of the eigenstates. In 1960, however, Wannier[7] proposed that in a real semiconductor with finite bands, a series of discrete energy levels should exist with an equidistant energetic spacing eFa that only depends on the field F and the periodicity a of the crystal in the direction of the field. This Wannier-Stark ladder was supposed to be the frequency domain counterpart of the Bloch oscillations (coherent field-induced oscillations of the band electrons between the band edges, both in a real and a k-space picture), which had been predicted long before.[8] The existence of the WS ladder and Bloch oscillations has been extensively discussed over many years in view of possible interband tunneling and scattering mechanisms destroying the wave function coherence. The discussion was supported by the fact that no reliable observation of WS levels has ever been reported in bulk material. In 1987, Emin and Hart,[9] however, concluded that at least interband tunneling should not suppress the observability of the WS ladder in interband absorption experiments.

Meanwhile, improved epitaxial growth techniques made it possible to fabricate one-dimensional artificial

superlattices, the lattice constant of which is increased by one or two orders of magnitude as compared to the bulk material and the bandwidths of which are decreased by a similar amount. In such structures both the spacing of the WS levels, which is now proportional to the superlattice period d, and the mean carrier scattering times are strongly enhanced, making the conditions for the observability of WS transitions and Bloch oscillations more favorable. In 1988, Mendez *et al.*[10] clearly identified WS transitions in the photocurrent spectra of $GaAs/Al_{0.35}Ga_{0.65}As$ superlattices. In 1992, Bloch oscillations were detected in the time domain in optical four wave mixing experiments on similar samples.[11,12]

FK oscillations can be less easily observed in the absorption spectra of superlattices, due to the small miniband widths and the minuteness of the structures. However, in 1992, Schneider *et al.*[13] succeeded in the detection of FK oscillations at the lower miniband edge of a strongly coupled GaAs/AlAs superlattice for low electric fields. In the high-field range, the same sample showed the usual WS transitions.

Until recently, detailed investigations on the transition from the FK to the WS regime were lacking. Callaway had shown theoretically[14] that the FK absorption spectra of bulk semiconductors should have an additional modulation, due to WS transitions. Bleuse *et al.*[15] demonstrated that FK oscillations should be obtained from the WS absorption spectra of a superlattice in the low-field limit. Both of them only considered the lower (mini-) band edge and there was no clear idea about the interference between the FK oscillations from the lower and upper (mini-) band edges and the WS transitions. Recently, however, we succeeded in analyzing superlattice absorption spectra over an energy range covering the complete lowest combined heavy hole-electron miniband width and over a field range from the FK to the WS limit.[1] A clear interplay between both kinds of structure could be demonstrated and the origin of that structure could be revealed. This paper is intended to provide a detailed theoretical description of our ideas and further experimental evidence for our conclusions.

II. PRELIMINARY CONSIDERATIONS

The electronic properties of periodic semiconductor superlattices depend strongly on the composition and the width of the barrier material. If the coupling between the wells is strong enough, the discrete levels of the single quantum wells split into minibands. In the zero-field case, the idealized wave functions are the completely delocalized Bloch functions of the artificial superlattice. If an electric field is applied parallel to the growth direction, the degeneracy of the QW levels is removed and the quasicontinuum of miniband Bloch states transforms into a series of levels with an equidistant energy spacing eFd, which is due to the discrete translation symmetry of the (infinite) lattice. At the same time, the wave functions become localized within a range $\Lambda = \Delta E^B/(eF)$ [ΔE^B: (mini-) bandwidth] centered around a certain well n. In Fig. 1(a), the situation close to a complete localization of

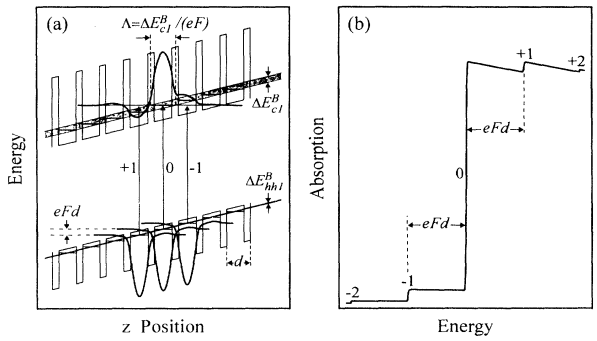

FIG. 1. Schematic drawing of (a) potential profile and WS states and (b) absorption spectra of a semiconductor superlattice with an electric field applied parallel to the growth direction. For clarity, only the lowest conduction ($c1$) and uppermost heavy hole (hh1) miniband (shaded areas) and a few of the associated WS states are shown. Possible light-induced transitions are indicated by arrows in (a).

both electron and hole wave functions is shown schematically. If the localization length Λ is much larger than d, it defines the width of the carrier motion between the tilted (mini-) band edges, which are the turning points of the semiclassical carrier motion.

The intensity of the transition from hole level m to electron level n is proportional to the square of the overlap between the corresponding wave functions. It usually has its maximum value for the spatially direct transitions $m = n$ and decreases monotonously with increasing value of $|m - n|$. Since all transitions with equal $\rho = m - n$ are equal in energy, the energetic spectrum will reflect the WS-ladder energies. Each WS level forms a two-dimensional (2D) subband of states, with respect to the in-plane motion. The absorption spectra will, therefore, consist of a series of transitions with quasi-two-dimensional character [Fig. 1(b)]. The above mentioned hierarchy in WS transition intensities shall be called the "classical" WS effect and it will be shown that it is valid in the "high-" field case only (the term "high" is to be defined later). Actually this will be a crucial point in our line of argument.

The WS ladders can only exist if the carrier scattering times τ_s are large enough to permit at least one full Bloch oscillation cycle for the carriers accelerated by the field. Since the Bloch period $\tau_B(F) = h/(eFd)$ is inversely proportional to the field F, there must always exist a low-field limit in which a carrier accelerated from the lower miniband edge will be scattered before it reaches the upper miniband edge and even before it traverses those regions of the miniband in which the parabolic approximation for the dispersion around the minimum is still valid. As in the theory of the bulk FK effect, a description of the wave functions, in terms of envelope functions with respect to the superlattice cell, should be applicable [Fig. 2(a)] replacing the full superlattice wave function used in the WS case. In this limit, FK oscillations similar to bulk material will be observed, but with

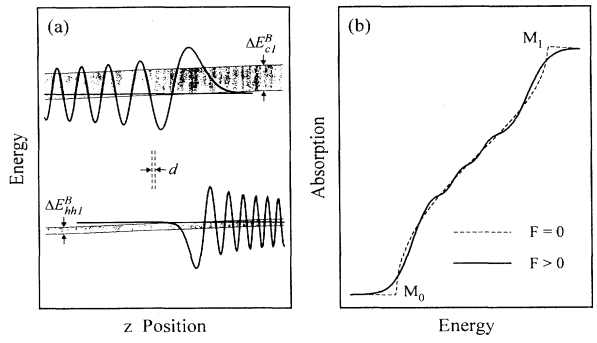

FIG. 2. (a) Superlattice minibands and envelope functions in the low-field limit. The lattice period d is small compared to the oscillation periods of the wave functions. (b) Superlattice absorption in the low-field limit showing FK oscillations near the lower (M_0) and the upper (M_1) combined miniband edge.

an oscillation period that corresponds to the effective miniband masses. Furthermore, these oscillations appear both near the lower and upper combined miniband edges [Fig. 2(b)]. However, in the absence of scattering events, the WS ladder will still be present. The influence of scattering processes in absorption spectra basically results in line broadening. Thus, it becomes clear that there has to be a relation between the WS and FK effect and that, in particular, the transition from one to the other is governed by the relation between the line broadening and the distance of the WS levels.

Experimentally WS transitions and FK oscillations can be distinguished easily using their field dependences. WS transitions originate at the center-of-mass energy of the combined miniband and move linearly towards the miniband edges with increasing field [Fig. 3(a)]. The structures due to FK oscillations, on the other hand, originate at the miniband edges and move in the direction of the center with a characteristic nonlinear $F^{2/3}$ behavior [Fig. 3(b)].

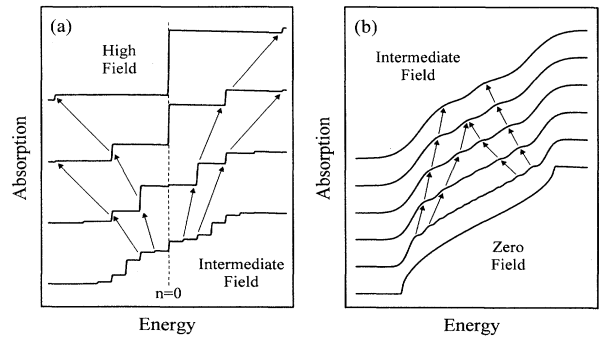

FIG. 3. Schematic drawing of (a) WS absorption spectra in the range from high to intermediate electric fields and (b) FK absorption spectra in the intermediate- to zero-field range. The field dependence of both kinds of structures is different (indicated by the arrows), making an experimental distinction possible.

III. THEORY

Our following considerations will in most parts be general, so they will be applicable to bulk semiconductors and insulators, as well as to semiconductor superlattices. The explicit results for the wave functions and absorption spectra, however, are calculated for a superlattice consisting of 11 ML (= 31.3 Å) wide GaAs wells and 1 ML (= 2.83 Å) wide AlAs barriers. In a subsequent section, these results will be compared to experiments on a superlattice sample with the same nominal parameters. We will first discuss the properties of the wave functions corresponding to the WS levels and then calculate the absorption spectra.

A. Wannier-Stark eigenstates

There has been a variety of approaches to calculate the wave functions of a periodic crystal in an electric field. In the crystal momentum representation, the time independent Schrödinger equation for the envelope function component in field direction (which is assumed to be the z direction) reads[16]

$$\left(E_n(k_z) - E_{n\nu} + ieF\frac{\partial}{\partial k_z}\right) A_{n\nu}(k_z) + ieF\sum_{n'} X_{nn'}(k_z) A_{n'\nu}(k_z) = 0, \tag{1}$$

where $A_{n\nu}(k_z)$ are the coefficients of the field-dependent eigenstates (Kane functions) $|\Psi_{n\nu}\rangle$ belonging to a (mini-) band n, expanded in the Bloch states $|\phi_{nk_z}\rangle$ of the (super-) lattice (lattice period d),

$$|\Psi_{n\nu}\rangle = \sum_{k_z} A_{n\nu}(k_z)\,|\phi_{nk_z}\rangle. \tag{2}$$

$E_n(k_z)$ is the dispersion of the (mini-) band n and $X_{nn'}(k_z)$ are the tunneling matrix elements defined by

$$X_{nn'}(k_z) = \int u^*_{nk_z}(z)\frac{\partial}{\partial k_z} u_{n'k_z}(z)\,dz, \tag{3}$$

where

$$\phi_{nk_z}(z) = e^{ik_z z} u_{nk_z}(z). \tag{4}$$

In a (super-) lattice that satisfies inversion symmetry with respect to the field direction, $X_{nn}(k_z)$ is identical to zero.[18] If all the remaining tunneling terms $X_{nn'}(k_z)$ are neglected, a solution of Eq. (1) can easily be obtained:[16]

$$A_{n\nu}(k_z) = \frac{1}{\sqrt{N}} \exp\left[\frac{i}{eF}\int_0^{k_z} [E_n(k'_z) - E_{n\nu}]\,dk'_z\right]. \tag{5}$$

$E_{n\nu}$ is the energy of the WS level ν:

$$E_{n\nu} = E_{n0} + \nu eFd, \tag{6a}$$

$$E_{n0} = \frac{d}{2\pi}\int_{-\pi/d}^{+\pi/d} E_n(k'_z)\,dk'_z, \tag{6b}$$

and N is the number of unit cells.

The shapes of the wave functions can be discussed more clearly if they are expressed in terms of (super-) lattice Wannier functions defined by

$$a_{n,p}(z) = \frac{1}{\sqrt{N}} \sum_{k_z} e^{-ik_z pd} \phi_{nk_z}(z). \tag{7}$$

Using

$$\phi_{nk_z}(z) = \frac{1}{\sqrt{N}} \sum_{p} e^{ik_z pd} a_{n,p}(z) \tag{8}$$

and Eq. (5), one obtains from Eq. (2),

$$\Psi_{n\nu}(z) = \sum_{p} \psi_{n\nu}(pd)\, a_{n,p}(z), \tag{9}$$

with

$$\psi_{n\nu}(pd) = \frac{1}{N} \sum_{k_z} \exp\left(\frac{i}{eF} \int_0^{k_z} [E_n(k_z') - E_{n\nu} + peFd]\, dk_z' \right). \tag{10}$$

Keeping in mind that the Wannier function $a_{n,p}(z)$ is strongly localized inside the well p and $a_{n,p}(z-d) = a_{n,p+1}(z)$, it is obvious that the behavior of the Kane function $\Psi_{n\nu}$ is determined by the envelope coefficients $\psi_{n\nu}(pd)$, which modulate the periodic series of Wannier functions $a_{n,p}$. In fact, Eq. (10) is the envelope function representation of the problem on the level of the (super-) lattice cell, which is, for bulk material, equal to the usual formalism.[17]

In the calculations for the superlattice investigated here, a rectangular shape of the superlattice potential has been assumed, and a Kronig-Penney model has been used to obtain the miniband dispersion and the Wannier functions. The properties of the host materials are described within an effective mass approximation for both electrons and holes neglecting Γ-X and Γ-L mixing. All results given here correspond to the lowest electron ($c1$) and the uppermost hole minibands (hh1, lh1), respectively. The calculation parameters are summarized in Table I, the calculated miniband parameters and transition energies in Table II.

In Fig. 4, the field-free superlattice potential, the calculated $E(k_z)$ dispersions for the lowest conduction miniband $c1$ and the uppermost heavy hole miniband hh1, and the corresponding Wannier functions are shown. The incomplete localization results from the k_z dependence of the Bloch functions u_{nk_z} which, in turn, depends on the extent of the deviation of the real band structure (solid lines) from the tight-binding limit (dashed lines). The influence of this effect on the absorption spectra, however, turns out to be small, even in our case of a strongly coupled superlattice.

The Kane functions for the lowest electron miniband $c1$ for various values of the electric field are shown in Fig. 5. The discussion can be restricted to $\Psi_{c1,\nu=0}$, since $\Psi_{n\nu}(z) = \Psi_{n0}(z - \nu d)$ [which can be easily verified by direct calculation using Eqs. (9), (10), and (6a), assuming an infinite superlattice]. One immediately recognizes (most easily visible for the low field values) that the wave functions consist of a lattice periodic part and an envelope. In the high field limit, the wave function $\Psi_{c1,0}$ is strongly centered around the well $p = 0$ and the amplitudes decrease with increasing distance from that well. This is the "classical" behavior of Kane functions. With decreasing fields, however, the spatial extension increases and the envelope $\psi_{c1,0}(pd)$ undergoes oscillations both as a function of the spatial position pd and the electric field. In consequence, the wave function no longer reaches its maximum value in the center well $p = 0$, but can even have zero crossings there for certain values of the electric field. This is also true for any other well. In this way, a complicated distribution of the electron density is obtained, which is far from the classical WS limit. For low fields the maximum values are even near the limits of the localization interval. This corresponds to a quasiclassical motion of the electron oscillating between the tilted band edges. In the vicinity of the turning points, the probability density is enhanced, because of the reduced carrier velocity.

We shall consider this low-field limit in some more detail. For a given eigenstate $\Psi_{c\nu}$, the exponential in Eq. (10) has a stationary phase if

TABLE I. Parameters used in the calculations.

d (GaAs) (Å)	31.09
d (AlAs) (Å)	2.83
m_c (GaAs) (m_0)	0.0665
m_c (AlAs) (m_0)	0.1495
m_{hh} (GaAs) (m_0)	0.3774[a]
m_{hh} (AlAs) (m_0)	0.5076[a]
m_{lh} (GaAs) (m_0)	0.0905[b]
m_{lh} (AlAs) (m_0)	0.2208[b]

[a] $m_{hh} = \frac{1}{\gamma_1 - 2\gamma_2}$, γ_1 and γ_2 being the Luttinger parameters for GaAs and AlAs.
[b] $m_{lh} = \frac{1}{\gamma_1 + 2\gamma_2}$.

TABLE II. Calculated miniband parameters and transition energies for the investigated 11/1 ML GaAs/AlAs superlattice.

n	$c1$	hh1	lh1
ΔE_n^B (eV)	0.332	0.050	0.249
E_n^l (eV)[a]	0.076	-0.033	-0.042
E_n^u (eV)[a]	0.408	-0.083	-0.292
E_{n0} (eV)[a]	0.208	-0.054	-0.140
m_n^l (m_0)	0.0765	-0.4415	-0.1045
m_n^u (m_0)	-0.0119	0.1241	0.0143
$\epsilon_{c1,n}^l$ (eV)		1.621	1.631
$\epsilon_{c1,n}^u$ (eV)		2.003	2.212
$\epsilon_{c1,n}^{00}$ (eV)		1.774	1.860

[a] Energy values with respect to the corresponding band edge of GaAs.

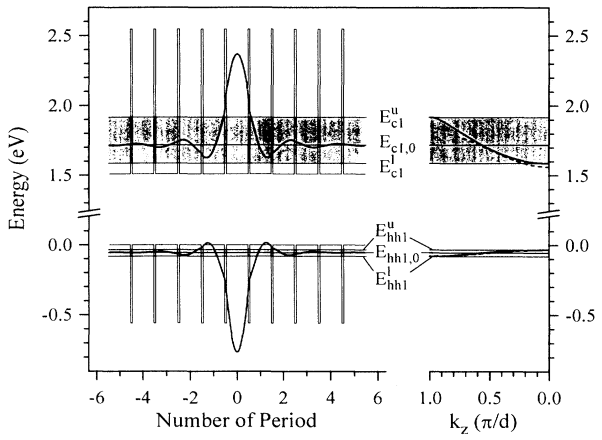

FIG. 4. Potential profile, Wannier functions $a_{c1/hh1,0}$ and $E(k_z)$ dispersions for the lowest electron ($c1$) and the uppermost heavy hole (hh1) miniband of the investigated 11/1 ML GaAs/AlAs superlattice. The $c1$ dispersion obtained by the Kronig-Penney model (solid line) deviates significantly from the corresponding tight-binding dispersion (dashed line).

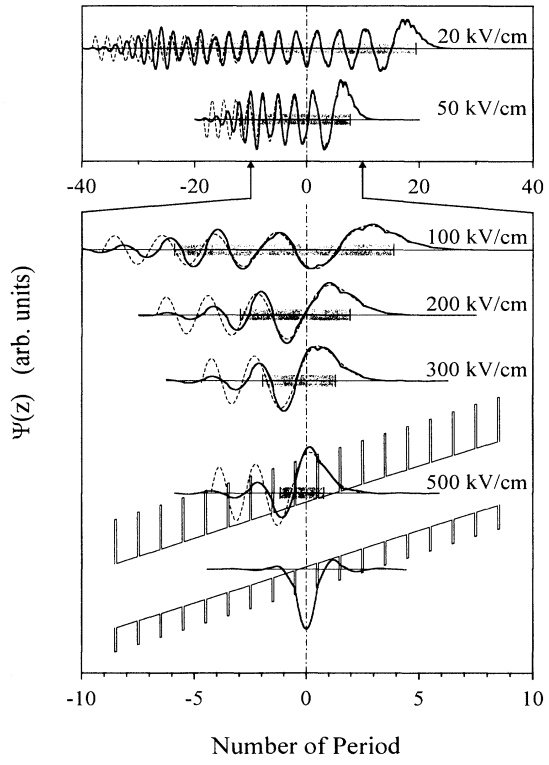

FIG. 5. Wave functions belonging to the ($\nu = 0$)-WS level of the $c1$ miniband of the investigated 11/1 ML GaAs/AlAs superlattice for various values of the field (solid lines). For comparison, the envelopes of the parabolic dispersion approximation near the lower miniband edge are shown (dashed lines). The miniband range is marked by gray bars. In the lower part of the figure, the superlattice potential and the ($\nu = 0$)-hh1 wave function for the highest-field value is included.

$$E_n(k_z) - E_{n\nu} + peFd = 0. \tag{11}$$

Hence, those values of k_z, which closely fulfill Eq. (11), will yield the maximum contribution to the sum in Eq. (10); all other values correspond to rapidly oscillating parts of the exponential, which cancel out due to the summation. For the following, we will assume inversion symmetry for the crystal, i.e., $E_n(-k_z) = E_n(k_z)$. If in this case, $E_{n\nu} - peFd$ is close to a band extremum at $k_z = 0$ [which is, for the lowest (mini-) band, the lower (mini-) band edge E_n^l; the above condition is also equivalent to pd being close to the corresponding classical turning point, cf. Fig. 1(a)], $E_n(k_z)$ can be expanded into a Taylor series up to second order giving

$$E_n(k_z) \approx E_n^{(0)} + \frac{\hbar^2 k_z^2}{2m^{(0)}}, \quad \text{with} \quad E_n^{(0)} = E_n(0), \tag{12}$$

which is the effective mass approximation around the critical point $k_z = 0$, $m^{(0)}$ being the effective (mini-) band mass. Note that $m^{(0)}$ can have a negative sign depending on the type of critical point. The integration in Eq. (10) can be carried out yielding

$$\psi_{n\nu}(pd) = \frac{1}{N}\sum_{k_z} \exp\left\{ i \left[\frac{\hbar^2}{2m^{(0)}eF}\frac{1}{3}k_z^3 + \left(\frac{E_n^{(0)} - E_{n\nu}}{eF} + pd \right) k_z \right] \right\}. \tag{13}$$

The summation over k_z has, in principle, to be carried out over the first Brillouin zone only. However, as discussed above, only small k_z values will contribute significantly and the sum can be extended to infinity. Transforming to an integral and changing variables leads to

$$\psi_{n\nu}(pd) \approx \frac{eFd}{2\pi\hbar\Theta^{(0)}} \times \int_{-\infty}^{+\infty} \exp\left\{ i \left[\frac{1}{3}q_z^3 + \frac{peFd - (E_{n\nu} - E_n^{(0)})}{\hbar\Theta^{(0)}} q_z \right] \right\} dq_z, \tag{14}$$

which is proportional to the integral representation of the Airy function,[19] yielding finally

$$\psi_{n\nu}(pd) \approx \frac{eFd}{\hbar\Theta^{(0)}} \,\mathrm{Ai}\left(\frac{peFd - (E_{n\nu} - E_n^{(0)})}{\hbar\Theta^{(0)}} \right), \tag{15}$$

with the electrooptic energy

$$\hbar\Theta^{(0)} = \left(\frac{(eF\hbar)^2}{2m^{(0)}} \right)^{1/3}. \tag{16}$$

(Here and below, $\hbar\Theta$ is defined as having the sign of the effective mass m.) This result is exactly equal to that obtained for the field-dependent envelope functions in the effective mass approximation, assuming infinitely extended parabolic bands.[18]

In bulk material, the envelope function ψ_{n0} is often treated as a continuous function averaging over the fine structure, due to the Wannier functions. In analogy, the approximation Eq. (14) for $\psi_{n0}(z)$ for the case of our superlattice is included in Fig. 5, where z is assumed to be continuous (dashed lines). Since only the envelope is shown, the lattice periodic parts are suppressed and the wave functions smoothed out, but the essential shapes of the wave functions remain unchanged. As expected, the approximation Eq. (14) is very good in the vicinity of the low-energy classical turning point (positive z values) for low-field values, where the complete Kane states, as well as the oscillation periods of the envelope $\psi_{n0}(z)$, are extended over many superlattice periods. However, it is interesting to note that it does not become too bad even in the case of high fields and strongly localized wave functions.

An analogous treatment can be applied to a band extremum at $k_z = \pm\pi/d$ [which is, for the lowest (mini-) band, the upper (mini-) band edge E_n^u]. If $E_{n\nu} - peFd$ is close to that point, $E_n(k_z)$ can be expanded,

$$E_n(k_z) \approx E_n^{(1)} + \frac{\hbar^2 \left(\frac{\pi}{d} - k_z\right)^2}{2m^{(1)}},$$

with

$$E_n^{(1)} = E_n(\pi/d), \tag{17}$$

where $m^{(1)}$ is the effective (mini-) band mass at that (mini-) band edge. The coefficient function $\psi_{n\nu}(pd)$, in this case, is given by (see Appendix A)

$$\psi_{n\nu}(pd) \approx \frac{eFd}{\hbar\Theta^{(1)}}(-1)^{p+\nu}\mathrm{Ai}\left(\frac{peFd - (E_{n\nu} - E_n^{(1)})}{\hbar\Theta^{(1)}}\right), \tag{18}$$

with

$$\hbar\Theta^{(1)} = \left(\frac{(eF\hbar)^2}{2m^{(1)}}\right)^{1/3}. \tag{19}$$

Again the main part is the Airy function establishing the semiclassical Franz-Keldysh limit. There is an additional change of the sign for every step from one to the next lattice site, which reflects the behavior of the Bloch functions around $k_z = \frac{\pi}{d}$ that are the main constituents of the Kane functions in the vicinity of the considered band extremum. This behavior is clearly visible at the high-energy classical turning point (positive z values) for the wave functions in Fig. 5. It was neglected in the original treatment of the FK effect, because the derivation based on a real space Wannier equation was implicitly restricted to band extrema at $\mathbf{k} = 0$. However, this does not affect the results of the dielectric function, as we will show below.

From Eq. (10), one can also derive an expression for the approximate spatial extension of the Kane states. The values of $\psi_{n\nu}(pd)$ remain high, as long as the exponential has a point of stationary phase. This is the case for

$$\frac{E_n^l - E_{n0}}{eFd} \le (\nu - p)d \le \frac{E_n^u - E_{n0}}{eFd}. \tag{20}$$

If $(\nu - p)d$ is outside this range, the amplitude $\psi_{n\nu}(pd)$ will drop off rapidly. This result confirms our previous considerations about the extension of the wave functions resulting from a classical picture of carrier motion. Due to the pronounced asymmetry of the miniband dispersion, with respect to $E_{c1,0}$, i.e., $E_{c1}^u - E_{c1,0} > E_{c1,0} - E_{c1}^l$ (cf. Table II), the extension of $\Psi_{c1,0}$ in the negative z direction is larger than in the positive z direction. This is also obvious in Fig. 5.

B. Absorption spectra

In order to discuss the optical absorption spectra, one can assume as a first approximation that the hole wave functions are mostly localized inside one well for the most relevant field range. This is a good approach for the heavy holes, the Kane functions of which become strongly localized at comparatively low fields, due to their small miniband width resulting from the high effective mass. However, as shown below, the essential results of the following discussion will not be affected even if this approximation fails. It will, therefore, also be valid for the light holes with certain modifications.

Under the present assumption, the oscillator strength of a certain WS transition $\mu \to \nu$, which is proportional to the square of the overlap integral of the hole and the electron wave function, is only determined by the square of the electron wave function $\Psi_{c\nu}$ in the well μ, that is the envelope $|\psi_{c\nu}(\mu d)|^2$. The spectrum of the optical transitions, therefore, is mostly an image of the shape of the electron wave functions.

A direct calculation of the absorption for one pair of electron and hole (mini-) bands (labeled by c and v) yields

$$\alpha_{cv}(\omega) \propto \frac{1}{\omega}\frac{1}{Nd}\sum_{\rho \le \frac{\hbar\omega - \epsilon_{cv}^{00}}{eFd}} N|\mu_{cv}(\rho)|^2, \tag{21}$$

where the transition amplitudes $\mu_{cv}(\rho)$ are

$$\mu_{cv}(\rho) = \frac{1}{N}\sum_{k_z}\langle u_{ck_z}|u_{vk_z}\rangle \times \exp\left\{\frac{i}{eF}\int_0^{k_z}\left(\epsilon_{cv}(k_z') - \epsilon_{cv}^{00} - \rho eFd\right)dk_z'\right\}, \tag{22}$$

with

$$\epsilon_{cv}^{00} = E_{c0} - E_{v0}, \tag{23a}$$

$$\epsilon_{cv}(k_z') = E_c(k_z') - E_v(k_z'), \tag{23b}$$

and an energy-independent two-dimensional in-plane density of states has been assumed.

In the case of tight-binding (mini-) bands,

$$\epsilon_{cv}(k_z) = \epsilon_{cv}^{00} - \frac{\Delta E_{cv}^B}{2}\cos(k_z d), \tag{24}$$

where ΔE_{cv}^B is the combined electron-hole (mini-) band width, the overlap integral of the Bloch functions $\langle u_{ck_z}|u_{vk_z}\rangle$ is constant, and Eq. (22) reduces to a Bessel function:[20,15]

$$\mu_{cv}(\rho) = \mathrm{J}_\rho\left(\frac{\Delta E_{cv}^B}{2eFd}\right). \tag{25}$$

If, in general, the small and monotonous variation of $\langle u_{ck_z}|u_{vk_z}\rangle$ with k_z is neglected, the expression for $\mu_{cv}(\rho)$ obviously has exactly the same shape as that for the wave function coefficients $\psi_{n0}(pd)$ in Eq. (10), except that the one-(mini-) band energies $E_n(k_z)$ and E_{n0} have to be exchanged for the inter-(mini-) band energies $\epsilon_{cv}(k_z)$ and ϵ_{cv}^{00}. Therefore, the above discussion for the squares of the envelope coefficients $|\psi_{n0}(pd)|^2$ can immediately be applied to the oscillator strengths of the WS transitions.

Figure 6 shows a plot of spectra of the differential absorption $\partial\alpha(\omega)/\partial\omega$ over a wide field range for the 11 ML/1 ML GaAs/AlAs superlattice discussed here, calculated with the use of Eqs. (21) and (22). A finite Gaussian broadening (FWHM = 24 meV) has been added,

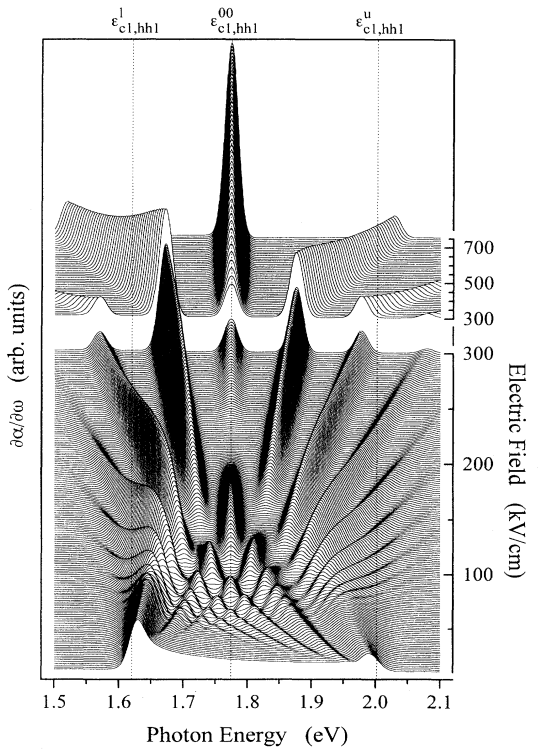

FIG. 6. Calculated differential absorption spectra $\partial\alpha/\partial\omega$ for the c1-hh1 transitions of the investigated superlattice for a broad range of fields. $\epsilon^{l}_{c1,hh1}$, $\epsilon^{u}_{c1,hh1}$, and $\epsilon^{00}_{c1,hh1}$ are the positions of the lower and the upper combined miniband edge and the $\rho = 0$—WS transition.

which has a similar amount as that observed in the experimental spectra. The differential absorption has been plotted instead of the absolute values in order to resolve the structures more clearly. Only the lowest electron (c1) and the uppermost heavy hole miniband (hh1) have been taken into account. Due to the strong interwell coupling, the electron miniband has a width of $\Delta E_{c1}^B = 332$ meV, the heavy hole miniband yet $\Delta E_{hh1}^B = 50$ meV (Table II). As shown above (Fig. 4), the $E_n(k_z)$ dispersions are remarkably asymmetric, with respect to the lower and upper miniband edges, due to the use of the Kronig-Penney instead of a tight-binding model. Therefore, the "center of mass" of the minibands, which is equal to E_{c0}, respectively, E_{v0} defined by Eq. (6b), and the energy $\epsilon^{00}_{c1,hh1}$ of the $\rho = 0$—WS transition are shifted towards the Γ-point miniband edges. Also, the miniband effective masses at $k_z = 0$ are higher than at $k_z = \pi/d$ (cf. Table II), which causes an enhancement of transition strengths at the lower miniband edge, as compared to the upper one. Similar to the behavior of the wave functions, the transition strengths decay exponentially as soon as the transition energies are outside the combined miniband range. This is the reason why WS transitions cannot be resolved in superlattices with very small miniband widths, i.e., in multiple quantum well structures.

In a way similar to the behavior of the wave functions, the modulation of the WS transitions causes an infinite series of zeros of $\mu_{cv}(\rho)$, with a decreasing electric field for each transition ρ. The first zero occurs at a critical value $F_{\mathrm{crit}}(\rho)$ of the electric field, which can be estimated by using the tight-binding approximation (25) and calculating the first zero $x_1(\rho)$ of the Bessel function J_ρ,

$$F_{\mathrm{crit}}(\rho) \approx \frac{\Delta E_c^B + \Delta E_v^B}{2edx_1(\rho)}. \tag{26}$$

At a certain field value beyond $F_{\mathrm{crit}}(0)$, the "classical" hierarchy of WS transition strengths occurs (in our case at $F \approx 400$ kV/cm, cf. Fig. 6) and is retained for increasing field ("high-field range"). For decreasing field, a complicated distribution of transition intensities occurs. In order to show the field and energy dependence more clearly, the spectra in the lower part of Fig. 6 have been plotted again in the gray scale plot of Fig. 7.

The zeros of $\mu_{cv}(\rho)$ create a regular pattern (dashed lines) superimposed on the WS transitions (full lines), consisting of structures originating at the $\rho = 0$ transition and moving towards both the lower and upper miniband edges. In this way, a triangular section of the field-energy plane is formed—the energy axis making up its baseline—in which the modulation of the WS transitions occurs ("intermediate-field range"). From a certain value of the electric field, individual WS transitions cannot be resolved any longer (here for $F \lesssim 40$ kV/cm), due to finite level broadening. In this case, only the structure due to the modulation of the oscillator strengths, which changes more slowly with photon energy, remains ("low-field range"). This is also the situation in bulk crystals,

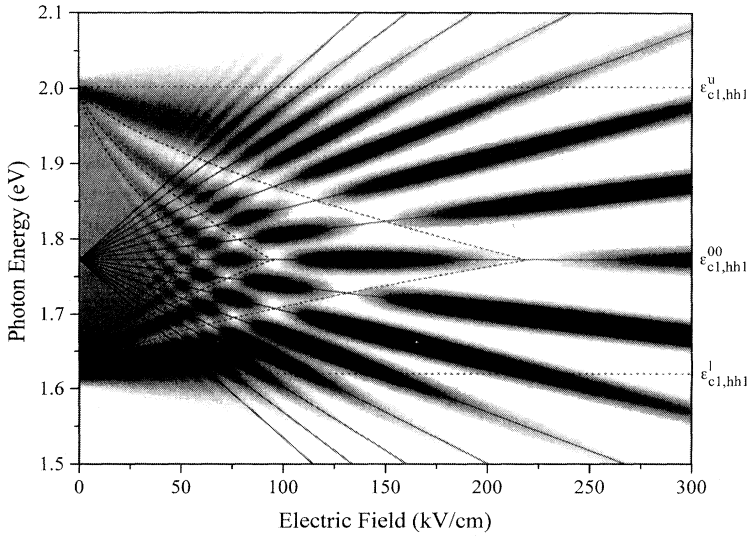

FIG. 7. Gray scale plot of the calculated differential absorption spectra in the coexistence regime of the WS and FK effects. Solid lines: fan of WS transitions; dashed lines: fan of FK oscillation minima both near the lower and upper combined miniband edges; dotted lines: combined miniband edges.

where no reliable observation of the WS ladder has been reported yet.

In order to discuss the low-field range, we assume an M_0 critical point at the lower and an M_1 critical point at the upper combined electron-hole miniband edges, i.e., the situation valid for the lowest electron and uppermost hole miniband. Again, we neglect the k_z dependence of $\langle u_{ck_z}|u_{vk_z}\rangle$. Then we can use an analogous treatment as applied to the wave functions near $k_z = 0$ to evaluate Eq. (21) and (22) and obtain for the absorption near the lower combined miniband edge,

$$\alpha_{cv}(\omega) \propto \frac{1}{\omega d} \sum_{\rho \le \frac{\hbar\omega - \epsilon^{00}_{cv}}{eFd}} \left(\frac{eFd}{\hbar\Theta^l}\right)^2 \times \mathrm{Ai}^2\left(\frac{-\rho eFd - (\epsilon^{00}_{cv} - \epsilon^{l}_{cv})}{\hbar\Theta^l}\right), \quad (27)$$

with

$$\hbar\Theta^l = \left(\frac{(eF\hbar)^2}{2\mu^l}\right)^{1/3}, \quad (28)$$

where ϵ^l_{cv} is the energy of the lower combined (mini-) band edge, $\mu^l = \left(1/m^l_c + 1/m^l_v\right)^{-1}$ the reduced effective (mini-) band mass at this point.

If we transform $\sum_\rho \ldots$ to $\int d\rho \ldots$, which is possible if the terms of the sum change slowly with ρ and the discrete nature of ρ is concealed by broadening, and change variables, we immediately obtain

$$\alpha_{cv}(\omega) \propto \frac{1}{\omega}\frac{eF}{(\hbar\Theta^l)^2}\int_{-\infty}^{\hbar\omega-\epsilon^l_{cv}} \mathrm{Ai}^2\left(-\frac{E}{\hbar\Theta^l}\right) dE. \quad (29)$$

Using[3]

$$\int^x \mathrm{Ai}^2(t)\,dt = x\mathrm{Ai}^2(x) - \mathrm{Ai}'^2(x), \quad (30)$$

we end up with

$$\alpha_{cv}(\omega) \propto \frac{1}{\omega}\frac{eF}{\hbar\Theta^l}\left[\mathrm{Ai}'^2(x) - x\mathrm{Ai}^2(x)\right], \quad (31)$$

where

$$x = \frac{\epsilon^l_{cv} - \hbar\omega}{\hbar\Theta^l}. \quad (32)$$

Furthermore, it is possible to show (Appendix B) that a similar relation holds for the upper combined (mini-) band edge:

$$\alpha_{cv}(\omega) \propto \frac{1}{\omega}\left(\frac{1}{d} - \frac{eF}{\hbar\Theta^u}\left[\mathrm{Ai}'^2(x) - x\mathrm{Ai}^2(x)\right]\right), \quad (33)$$

where

$$\hbar\Theta^u = \left(\frac{(eF\hbar)^2}{2\mu^u}\right)^{1/3}, \quad (34)$$

$$x = \frac{\epsilon^u_{cv} - \hbar\omega}{\hbar\Theta^u}. \quad (35)$$

Equations (31) and (33) are identical to the expressions of Aspnes,[18] for the FK absorption around an M_0 and M_1 critical point. We have derived them for the case that the steplike structure of the WS ladder is smoothed out by broadening (parameter Γ), leaving only those structures in the absorption spectra which are due to the energy dependence of the transition matrix elements $\mu_{cv}(\rho = \frac{\hbar\omega - \epsilon^{00}_{cv}}{eFd})$.

Figure 8 shows the field-induced changes of superlattice absorption for several values of the field calculated exactly (solid lines) and with the FK approximations for

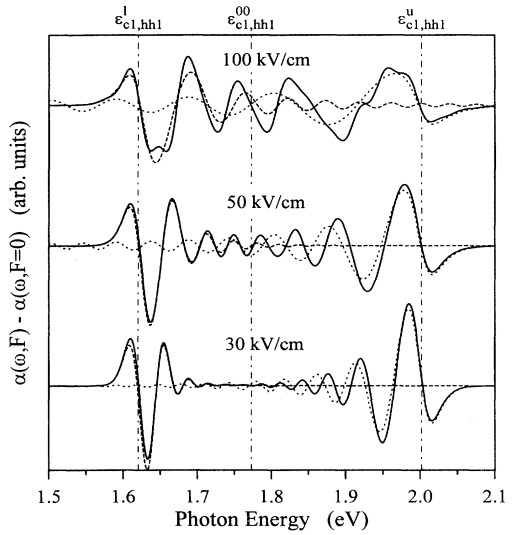

FIG. 8. Comparison between the calculated field-induced absorption changes in the exact model (solid lines) and the parabolic dispersion approximations for the lower (dashed lines) and the upper (dotted lines) combined miniband edge.

the lower [Eq. (31), dashed lines] and upper [Eq. (33), dotted lines] combined miniband edges. The approximations are good, as long as (i) the combined miniband dispersion $\epsilon_{cv}(k_z)$ can be considered parabolic and (ii) the broadening exceeds the spacing of the WS ladder. Both conditions are fulfilled for the low-field values at the lower combined miniband edge. At the upper miniband edge, the parabolic region of the dispersion is only small and deviations, due to dispersion nonparabolicity, occur.

The structure in Figs. 6 and 7 can now be interpreted as the WS transitions being modulated by FK oscillations. The zeros of the WS transition intensities are equivalent to the zeros of the FK oscillations. For decreasing fields, each WS transition is modulated by FK oscillations of steadily increasing order, originating either from the lower or the upper combined miniband edge. Vice versa, in the intermediate-field range ($\approx 40 \ldots 150$ kV/cm) the FK oscillations for a constant-field value exhibit fine structure resulting from the discrete WS transition energies. However, the series of the FK oscillations from the lower and the upper combined miniband edge do not interfere with each other as one would expect if the band edges could be treated independently. On the contrary, the two sets of FK oscillations move towards each other with increasing field and each pair of oscillation minima of the same order merges into one at a certain value of the field and ceases to exist for higher field values.

The positions of the first three minima of the FK oscillations, both near the lower and upper miniband edge, have also been marked in Fig. 7 by dashed lines illustrating this behavior. The energies have the characteristic $F^{2/3}$ dependence, which is obtained from keeping x in Eqs. (31)/(32) and (33)/(35) constant at the zeros of the Airy function. For the lower miniband edge, the use of the nominal effective masses gives a very good description for the position of the oscillation minima, even for higher electric fields. For the upper miniband edge, however, a modified miniband effective mass has to be used, since the parabolic approximation for the $E(k_z)$ dispersion is only valid in a small range around $k_z = \pm\pi/d$ (cf. Fig. 4).

In spite of the additional structure, due to the WS levels appearing for $eFd \gtrsim \Gamma$, the "envelope" of the absorption spectra still resembles the spectra obtained in the FK approximation. Thus, apart from the discrete nature of the WS transitions, the shape of the absorption spectra is entirely determined by the spectral dependence of the transition matrix elements $\mu_{cv}\left(\rho = \frac{\hbar\omega - \epsilon^{00}_{cv}}{eFd}\right)$, which, in turn, only depend on the (mini-) band dispersion and lead to the FK effect in the low-field limit. Therefore, we call this field-induced modulation of the transition matrix elements a *generalized Franz-Keldysh Effect.* This interpretation is supported by the fact that it is exactly this phenomenon that was addressed by Franz, Keldysh, and Aspnes, for the specific case of an infinite parabolic band dispersion.

IV. EXPERIMENTAL RESULTS

The measurements have been performed on a superlattice structure as discussed above, consisting of 80 periods of nominally 11 ML/1 ML GaAs/AlAs, sandwiched between a highly n-type doped $Al_{0.45}Ga_{0.55}As$ bottom layer and a highly p-type doped $Al_{0.45}Ga_{0.55}As$ top layer, grown on (100)-oriented n^+-GaAs substrate. A voltage U_{pn} was applied to contacts on top of the sample and on the n^+-GaAs substrate. Self-consistent potential calculations in a Thomas-Fermi model have confirmed the high accuracy (better than 1% for $U_{pn} < 0$ V, 10% for $U_{pn} < 1.2$ V) of a linear relation between the internal field and the applied voltage,

$$F = \frac{U_{bi} - U_{pn}}{ed_i}, \tag{36}$$

where $U_{bi} = 1.75$ V and $d_i = 2748$ Å.

The critical field for the transition to the classical WS limit for heavy hole-electron transitions, according to Eq. (26), is $F_{\text{crit}}(0) = 234$ kV/cm corresponding to a reverse bias of $U_{pn} = -4.7$ V. Thus, a broad range of intermediate fields, where the interference of WS transitions and their modulation by FK oscillations occurs, should be visible.

Figure 9(a) shows a set of absorption spectra for various values of the applied voltage obtained from photocurrent measurements at $T = 77$ K. For high reverse bias, a series of WS peaks can clearly be seen near the lower miniband edge and in the upper half of the miniband. From the energetic positions, they can be identified as hh1-c1 transitions. Light hole transitions cannot be observed in the field range investigated. This is reasonable, since they should be weaker by a factor of 3, due to the re-

spective values of the bulk momentum matrix elements. An additional factor of about 1.5 arises from the fact that the total oscillator strengths of the light hole transitions are distributed among the range of the combined electron-light hole miniband energies, which is about 1.5 times as large as that of the heavy holes.

For decreasing fields, the formerly monotonous changes of the WS transitions become now modulated by the FK-type oscillations. The first FK minimum can clearly be identified both near the lower and the upper combined miniband edges. The triangular section of interference between WS transitions and FK oscillations discussed above is obvious and marked by dashed lines in Fig. 9(a).

For comparison theoretical absorption spectra, including only hh1-c1 transitions, are shown in Fig. 9(b). The application of a Kronig-Penney model for the superlattice potential might be doubtful, since the assumption of rectangular barriers consisting of exactly one monolayer of pure AlAs may not be satisfied for the real structure. Schneider *et al.*,[13] however, have demonstrated for the same superlattice as considered in this work that the electronic structure is rather insensitive to the actual shape of the barrier, as long as the total barrier width d_b is small compared to the period and the integrated barrier potential $\int_{d_b} V(z)dz$ remains constant. Therefore, it is possible that our 1 ML AlAs barriers actually consist of, e.g., 3 ML of $Al_{0.33}Ga_{0.67}As$ or, more realistic, an alloy with continuously varying Al content, peaked at the nominal position of the barrier and smeared out over a few monolayers. However, since the positions of the miniband edges and the center of the miniband in the direct and the double differential (see below) absorption spectra are in good agreement with the theoretical values, we conclude that at least the effective barrier width in the sense of the integrated barrier potential has to be 1 ML. If, e.g., the real barrier widths were assumed to be 2 ML, the energies of the combined miniband edges would be $\epsilon^l_{c1,hh1} = 1.682\,\text{eV}$ and $\epsilon^u_{c1,hh1} = 1.899\,\text{eV}$, for the heavy hole transitions and $\epsilon^l_{c1,lh1} = 1.706\,\text{eV}$ and $\epsilon^u_{c1,lh1} = 2.049\,\text{eV}$, for the light hole transitions, which does not agree with the experimental data.

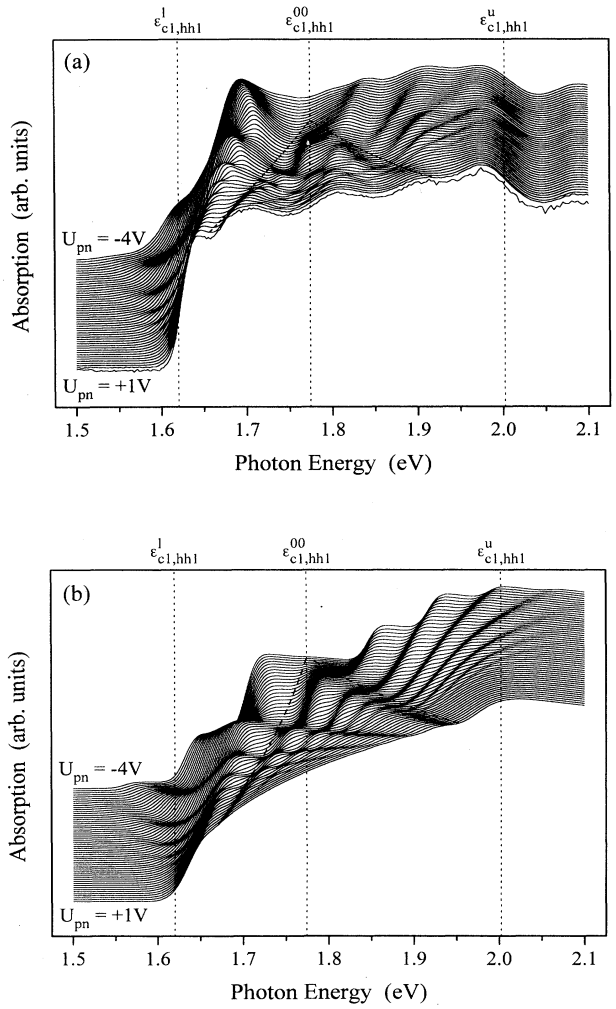

FIG. 9. Field-dependent experimental (a) and theoretical (b) absorption spectra for the investigated superlattice at T=77 K. The dashed lines indicate the region of coexistence of WS and FK effect for the c1-hh1 transitions.

As before, a Gaussian broadening function with FWHM = 24 meV has been used to mimic the experimental linewidth near the absorption threshold. The large value of the FWHM is probably due to small fluctuations of the effective well and barrier widths, which do not necessarily have to be integer multiples of 1 ML if alloy formation is assumed as discussed above. The interplay between WS transitions and FK oscillations observed in the experimental spectra are obvious in the theoretical spectra as well. However, the line shapes are somewhat different, in particular, in the vicinity of the lower absorption edge. This is due to excitonic effects,[21,22] which shall not be discussed here.

In the experimental absorption spectra, the WS and FK structure is superimposed on a large background absorption, making a clear identification of more than a few details difficult. Moreover, additional smooth oscillations are present, which result from optical resonances inside the layered structure and are nearly field independent. In order to eliminate these undesired structures, it is favorable to consider the second derivative of the absorption coefficient $\partial^2\alpha/(\partial\omega\partial F)$ (or the photocurrent), both with respect to the photon energy and the electric field. Such a signal can be measured directly by a recently developed modulation technique, the double differential photocurrent spectroscopy (DDPCS). In an appropriate experimental setup, both the voltage and the wavelength are modulated simultaneously by small ac components of different frequencies superimposed on certain dc values. The ac component of the photocurrent at the sum frequency, which is immediately proportional to the desired signal, is measured directly using lock-in technique. This method is extremely sensitive, since it does not require numerical or electronic differentiation of dc signals. The details of this technique will be described elsewhere.

A set of DDPC spectra and the corresponding theoret-

ical spectra are shown in the gray scale plots of Fig. 10. In both plots, the structures arising from WS transitions and FK oscillations are clearly visible and in excellent agreement. A symmetric fan of WS transitions from $\rho = -10$ to $\rho = +10$ (solid lines) can be identified outside the triangular coexistence region of FK and WS effect. Several periods of FK oscillations originating from both the lower and the upper miniband edges (dashed lines) are observed inside the coexistence region. As expected from the theory, there is a low-field range in which only the FK-type structure is observable (between $U_{pn} = 1.1$ V and 0.6 V), followed by an intermediate-field range with its characteristic superposition of FK oscillations and WS transitions. The high-field limit is beyond the accessible voltage range. Both in theory and experiment, the spatially direct WS transition (which corresponds to the "center of mass" energy of the miniband) is closer to the lower miniband edge, which reveals the deviations from tight-binding minibands. The difference in the slope of the lines tracing the positions of the FK minima near the lower and the upper miniband edges gives an additional hint for this conclusion. The slight redshift of the $\rho = 0$ WS transition, with increasing field, is partly due to the quantum confined Stark effect[23] (QCSE) inside the wells and partly to an increase of the excitonic binding energy as the character of the states transforms from 3D to 2D. The QCSE results from the inter-miniband coupling terms of Eq. (1), the excitonic effect is caused by the electron-hole Coulomb interaction. Both effects are not included in the calculations. Therefore, in our theory, the position of the $\rho = 0$ transition is strictly field independent.

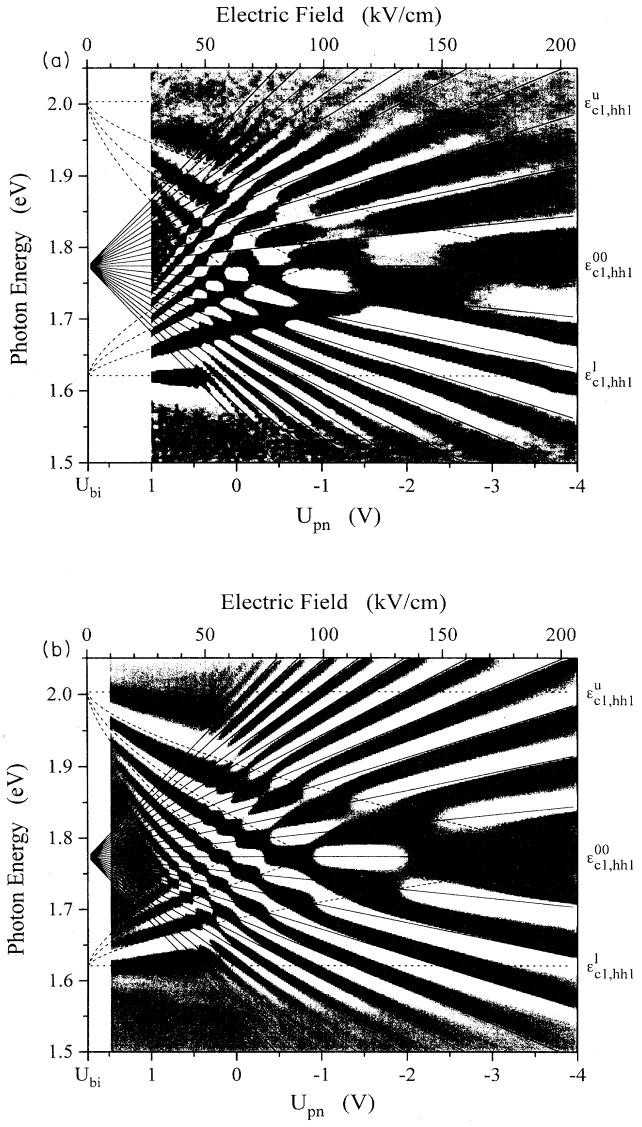

FIG. 10. Gray scale plot of the DDPC spectra (a) and the calculated $\partial\alpha^2/\partial\omega\partial F$ spectra (b) for the investigated superlattice. In both plots, the theoretical fan of WS transitions (full lines) and FK oscillations (dashed lines) and the combined miniband edges (dotted lines) are included.

The solid and dashed lines in the calculated as well as in the experimental spectra mark the *theoretical* positions of WS transitions and FK oscillations. In spite of the good general agreement, we note that the experimental energetic position of the structures is somewhat lower, in particular, in the upper half of the miniband. There is also a slight difference in the field values of corresponding structures between experimental and theoretical spectra. Both deviations indicate that the actual miniband widths are by some 10 meV smaller than calculated. The differences may arise from nonparabolicity effects of the bulk dispersions, as well as from somewhat larger effective barrier widths. Similar to the absorption spectra of Fig. 9, the structures in the lower half of the miniband are strongly enhanced in comparison with the upper half in the experimental spectra, whereas theory predicts comparable values. This is again an excitonic effect, which is due to the formation of bound states and a redistribution of oscillator strength to lower energies. However, excitonic effects do not significantly alter the WS transition energies and the positions of the FK oscillations on the energy scale relevant here, since the Coulomb energies are by nearly two orders of magnitude smaller than the combined miniband width.

V. CONCLUSIONS

We have investigated the electroabsorption characteristics of semiconductor superlattices with applied electric fields ranging continuously from the "miniband regime" to the "Wannier-Stark regime." It has been shown that a single-miniband crystal momentum representation, using the $E(k_z)$ dispersion of the superlattice as the dominant input parameter, is able to describe the structures observed in the absorption spectra over the whole field range.

In principle, Wannier-Stark transitions are present at any value of the field, even if their discrete nature is ob-

scured by level broadening. However, the classical hierarchy of transition intensities consisting of decreasing oscillator strengths, with increasing energetic distance from the $\rho = 0$ transition, is valid only in the high-field range. For lower fields, the transitions are modulated in a systematic way. When the spacing eFd of the WS levels becomes much smaller than the combined electron-hole miniband width $\Delta E_c^B + \Delta E_v^B$, the spectral dependence of the transition intensities obeys the expressions, as obtained for the Franz-Keldysh effect in the vicinity of the lower and upper combined miniband edge, corresponding to the case of an M_0 and an M_1 critical point, respectively. In consequence, pure Franz-Keldysh oscillations can be observed near the lower and upper combined miniband edges, as long as the broadening Γ inherent in the absorption spectra exceeds the spacing eFd of the Wannier-Stark levels (low-field range). This is completely the same situation as in bulk material, where Wannier-Stark transitions have never been observed thus far. It is physically equivalent to the picture that a carrier accelerated in the field is always far from completing one coherent Bloch oscillation cycle, because the mean scattering times are smaller than one Bloch period. In other words, the lower and upper miniband edges are decoupled with respect to carrier kinetics.

However, with increasing field, a situation can occur where the relation $\Gamma < eFd \ll \Delta E_c^B + \Delta E_v^B$ holds. In this regime, Wannier-Stark transitions can be resolved, but their intensities are modulated in a way characteristic for the Franz-Keldysh effect (intermediate-field range). This is the range of coexistence of the Wannier Stark and the Franz-Keldysh effect and covers a roughly triangular section of the field-energy plane. On the low-field side, its baseline coincides with the constant-field line $eFd = \Gamma$, on the high-field side its vertex is formed by the point, where the $\rho = 0$ transition has its last zero crossing, that is for $F = F_{\mathrm{crit}}(0)$ [Eq. (26)]. It should be emphasized that the low-field condition is not an intrinsic property of the electronic states. Thus, a coexistence regime of Franz-Keldysh and Wannier-Stark effect is, in principle, present in every superlattice, but may be unobservable due to broadening. Some further refinement of these conclusions may be necessary if the miniband widths are comparable to exciton binding energies,[24] but this is not considered in this work.

An obvious proof of our theoretical results has been given by optical experiments on a strongly coupled GaAs/AlAs superlattice. Due to the use of a highly sensitive technique of modulation spectroscopy, the double differential photocurrent spectroscopy, it has been possible to observe the theoretically expected structures clearly and with unprecedented resolution. In a continuous field range, Wannier-Stark transitions with indices between -10 and $+10$ have clearly been identified for high fields, as well as several periods of Franz-Keldysh oscillations originating from both the lower and the upper miniband edge for low fields. In the intermediate-field regime, the modulation of Wannier-Stark transitions by Franz-Keldysh oscillations or, vice versa, a fine structure of the FK oscillations, due to the Wannier-Stark transitions, is clearly visible. Excellent agreement with the theoretical simulations of the spectra has been found.

APPENDIX A

In this appendix, we derive Eq. (18) for the low-field limit of the coefficients $\psi_{n\nu}(pd)$ near a (mini-) band extremum at $k_z = \pi/d$. We start from Eq. (10) and immediately transform it into an integral representation

$$\psi_{n\nu}(pd) = \frac{d}{2\pi}\int_{-\pi/d}^{+\pi/d} \exp\left(\frac{i}{eF}\int_0^{k_z}[E_n(k_z') - E_{n\nu} + peFd]\,dk_z'\right)dk_z.$$

The outer integral can be split into two parts ranging from $-\pi/d$ to 0 and 0 to π/d. If the integration limits of the first part are shifted by $2\pi/d$, the result will be unaffected, as can be shown by direct calculation using Eq. (6b) and the fact that $E_n(k_z')$ is periodic with $2\pi/d$. We, therefore, change the integration limits to 0 to $2\pi/d$. The inner integral can be transformed to

$$\int_0^{k_z}[E_n(k_z') - E_{n\nu} + peFd]\,dk_z' = \int_{+\pi/d}^{k_z}[E_n(k_z') - E_{n\nu} + peFd]\,dk_z' + \int_0^{\pi/d}[E_n(k_z') - E_{n\nu} + peFd]\,dk_z'$$
$$= \int_{+\pi/d}^{k_z}[E_n(k_z') - E_{n\nu} + peFd]\,dk_z' + (p-\nu)eF\pi,$$

by the use of Eqs. (6a) and (6b). This leads to

$$\psi_{n\nu}(pd) = \exp[i\pi(p-\nu)]\,\frac{d}{2\pi}\int_0^{2\pi/d}\exp\left\{\frac{i}{eF}\int_{\pi/d}^{k_z}[E_n(k_z') - E_{n\nu} + peFd]\,dk_z'\right\}dk_z$$
$$= (-1)^{(p-\nu)}\,\frac{d}{2\pi}\int_{-\pi/d}^{+\pi/d}\exp\left\{\frac{i}{eF}\int_0^{k_z}\left[E_n\left(k_z' + \frac{\pi}{d}\right) - E_{n\nu} + peFd\right]\,dk_z'\right\}dk_z.$$

If Eq. (17) is inserted, a calculation analogous to the derivation of Eq. (15) from Eq. (13) yields Eq. (18).

APPENDIX B

Here, we derive Eq. (33) for the low-field limit of the absorption near an M_1 critical point at the upper combined miniband edge.

We first evaluate

$$\sum_{\rho}\left|\frac{1}{N}\sum_{k_z}\exp\left\{\frac{i}{eF}\int_0^{k_z}[\epsilon_{cv}(k_z')-\epsilon_{cv}^{00}-\rho eFd]\,dk_z'\right\}\right|^2$$

$$=\frac{1}{N^2}\sum_{k_{z_1},k_{z_2}}\exp\left\{\frac{i}{eF}\left[\int_0^{k_{z_1}}\epsilon_{cv}(k_{z_1}')\,dk_{z_1}'-\int_0^{k_{z_2}}\epsilon_{cv}(k_{z_2}')\,dk_{z_2}'+\epsilon_{cv}^{00}(k_{z_2}-k_{z_1})\right]\right\}\sum_{\rho}\exp[i\rho d(k_{z_2}-k_{z_1})]$$

$$=1,$$

since

$$\sum_{\rho}\exp[i\rho d(k_{z_2}-k_{z_1})]=N\delta_{k_{z_2},k_{z_1}}$$

(ρ and k_z can have N different values).

Using this result, Eq. (21) can be written as

$$\alpha_{cv}\propto\frac{1}{\omega d}\left(1-\sum_{\rho>\frac{\hbar\omega-\epsilon_{cv}^{00}}{eFd}}|\mu_{cv}^{(\rho)}|^2\right).$$

$\mu_{cv}^{(\rho)}$ can be calculated applying the procedure used in Appendix A, for the respective wave function. One obtains

$$\alpha_{cv}\propto\frac{1}{\omega d}\left[1-\sum_{\rho>\frac{\hbar\omega-\epsilon_{cv}^{00}}{eFd}}\left(\frac{eFd}{\hbar\Theta^u}\right)^2\mathrm{Ai}^2\left(\frac{\rho eFd-(\epsilon_{cv}^{00}-\epsilon_{cv}^{u})}{\hbar\Theta^u}\right)\right].$$

Transforming the sum over ρ into an integral, changing variables and using Eq. (30), one easily obtains Eq. (33).

[1] K.H. Schmidt, N. Linder, G.H. Döhler, H.T. Grahn, K. Ploog, and H. Schneider, Phys. Rev. Lett. **72**, 2769 (1994).

[2] W. Franz, Z. Naturforsch. Teil A **13**, 484 (1958); L.V. Keldysh, Zh. Eksp. Teor. Fiz. **34**, 1138 (1958) [Sov. Phys. JETP **34**, 788 (1958)].

[3] D.E. Aspnes, Phys. Rev. **147**, 554 (1966).

[4] D.E. Aspnes, Phys. Rev. **153**, 972 (1967).

[5] M. Cardona, in *Solid State Physics: Advances in Research and Applications*, edited by F. Seitz, D. Turnbull, and H. Ehrenreich (Academic Press, New York, 1969), Suppl. 11; see, also, Ref. 18.

[6] L.V. Keldysh, O.V. Konstantinov, and V.I. Perel, Fiz. Tekh. Poluprovodn. **3**, 1042 (1969) [Sov. Phys. Semicond. **3**, 876 (1970)].

[7] G.H. Wannier, Phys. Rev. **117**, 432 (1960).

[8] F. Bloch, Z. Phys. **52**, 555 (1928); C. Zener, Proc. R. Soc. London Ser. A **145**, 523 (1934).

[9] D. Emin and C.F. Hart, Phys. Rev. B **36**, 7353 (1987); L. Kleinman, *ibid.* **41**, 3857 (1990); D. Emin and C.F. Hart, *ibid.* **41**, 3859 (1990).

[10] E.E. Mendez, F. Agulló-Rueda, and J.M. Hong, Phys. Rev. Lett. **60**, 2426 (1988).

[11] J. Feldmann, K. Leo, J. Shah, D.A.B. Miller, J.E. Cunningham, T. Meier, G. von Plessen, A. Schulze, P. Thomas, and S. Schmitt-Rink, Phys. Rev. B **46**, 7252 (1992).

[12] K. Leo, P. Haring-Bolivar, F. Brüggemann, R. Schwedler, and K. Köhler, Solid State Commun. **84**, 943 (1992).

[13] H. Schneider, A. Fischer, and K. Ploog, Phys. Rev. B **45**, 6329 (1992).

[14] J. Callaway, Phys. Rev. **130**, 549 (1963); **134**, A998 (1964).

[15] J. Bleuse, G. Bastard, and P. Voisin, Phys. Rev. Lett. **60**, 220 (1988).

[16] E.O. Kane, J. Phys. Chem. Solids **12**, 181 (1959).

[17] J.M. Ziman, *Principles of the Theory of Solids*, 2nd ed. (Cambridge University Press, London, 1972).

[18] D.E. Aspnes and N. Bottka, in *Electric-Field Effects on the Dielectric Function of Semiconductors and Insulators*, edited by R.K. Willardson and A.C. Beer, Semiconductors and Semimetals, Vol. 9 (Academic Press, New York, 1972).

[19] M. Abramowitz and I.A. Stegun, *Handbook of Mathematical Functions* (Dover, New York, 1972).

[20] M. Saitoh, J. Phys. C **5**, 914 (1972).

[21] N. Linder, W. Geißelbrecht, G. Philipp, K.H. Schmidt, and G.H. Döhler, J. Phys. (France) IV **3**, C-195 (1993).

[22] N. Linder, K.H. Schmidt, W. Geißelbrecht, G.H. Döhler, H.T. Grahn, K. Ploog, H. Schneider, and K. Fujiwara, *Proceedings of the 22nd International Conference on the Physics of Semiconductors* (World Scientific, Singapore, 1995), p. 1484.

[23] See, e.g., G. Bastard, *Wave Mechanics Applied to Semiconductor Heterostructures* (Les Éditions de Physique, Les Ulix Cedex, 1989).

[24] A.M. Fox, D.A.B. Miller, J.E. Cunningham, W.Y. Jan, C.Y.P. Chao, and S.L. Chuang, Phys. Rev. B **46**, 15 365 (1992).

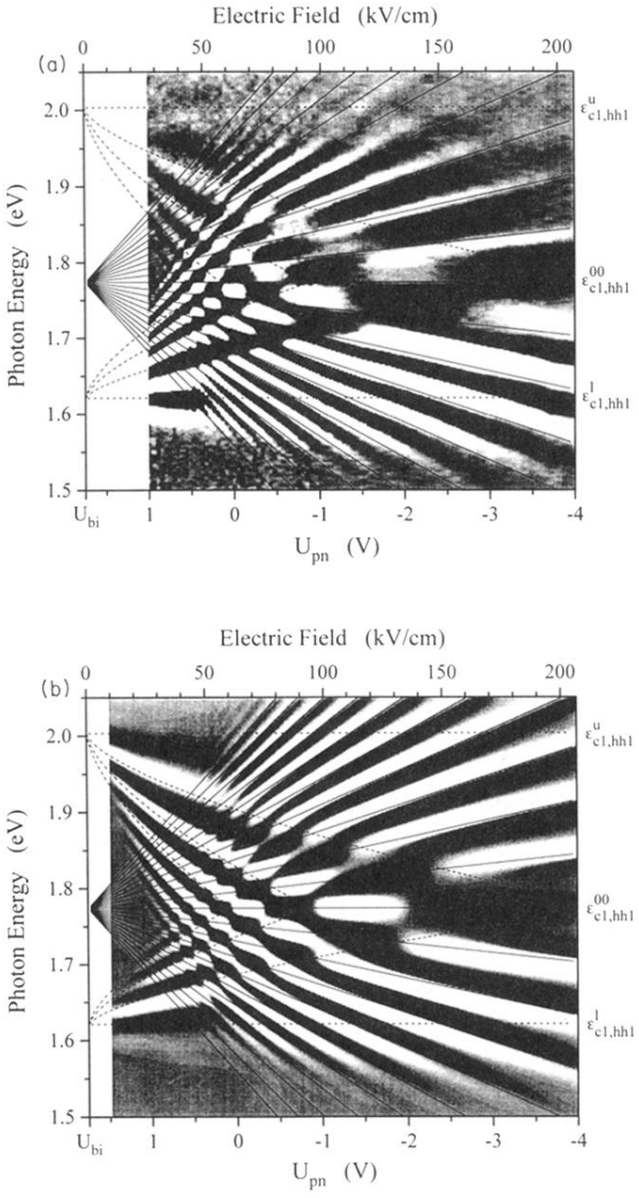

FIG. 10. Gray scale plot of the DDPC spectra (a) and the calculated $\partial\alpha^2/\partial\omega\partial F$ spectra (b) for the investigated superlattice. In both plots, the theoretical fan of WS transitions (full lines) and FK oscillations (dashed lines) and the combined miniband edges (dotted lines) are included.

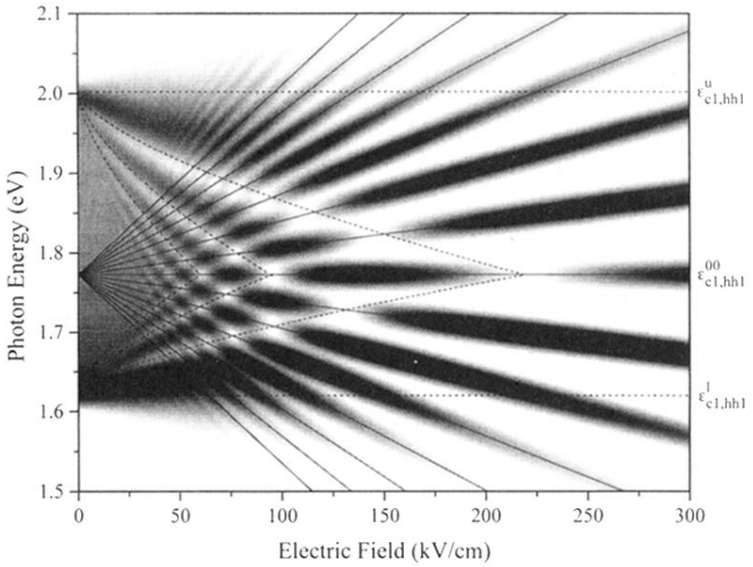

FIG. 7. Gray scale plot of the calculated differential absorption spectra in the coexistence regime of the WS and FK effects. Solid lines: fan of WS transitions; dashed lines: fan of FK oscillation minima both near the lower and upper combined miniband edges; dotted lines: combined miniband edges.